Biomimetic microelectronics for regenerative neuronal cuff implants

Article (Published Version)

Biomimetic Microelectronics for Regenerative Neuronal Cuff Implants

Daniil Karnaushenko, Niko Münzenrieder, Dmitriy D. Karnaushenko, Britta Koch, Anne K. Meyer, Stefan Baunack, Luisa Petti, Gerhard Tröster, Denys Makarov,* and Oliver G. Schmidt*

Living species possess the ability to adapt their shape during the life cycle, e.g., through growth, replication, healing, or motion. Imitating this behavior of nature archetypes, synthetic systems attain adaptability to environmental changes (e.g., artificial irises[1] adjust to the light intensity) as well as possibility to interact with the environment mechanically[2,3] or chemically.[4,5] Mimicking the mechanics of the plant cell swelling process in osmosis, the shape of soft objects can be tailored by using stimuli-responsive polymers.[6] In hydrogel composites,[7] a reversible shape transformation including elongation, twisting, or folding[8] is achieved upon external chemical or thermal stimulation rendering these biomimetic devices to be mechanically active. Although mechanically adaptive to the environment, these soft actuators do not carry active electronics to assess and communicate the environmental changes. Alternatively, there are ultrathin and lightweight mechanically flexible and even imperceptible electronics,[9–12] which are electrically active but lack of reversible self-actuation.

D. Karnaushenko, D. D. Karnaushenko, B. Koch, Dr. A. K. Meyer, Dr. S. Baunack, Dr. D. Makarov, Prof. O. G. Schmidt
Institute for Integrative Nanosciences
Institute for Solid State and Materials Research Dresden (IFW Dresden)
01069 Dresden, Germany
E-mail: d.karnaushenko@ifw-dresden.de; d.makarov@ifw-dresden.de

Dr. N. Münzenrieder, L. Petti, Prof. G. Tröster
Electronics Laboratory
ETH Zürich
Gloriastrasse 35, 8092 Zürich, Switzerland

Dr. N. Münzenrieder
Sensor Technology Research Center
University of Sussex
Falmer
Brighton, BN1 9QT, UK

Prof. O. G. Schmidt
Material Systems for Nanoelectronics
Chemnitz University of Technology
09107 Chemnitz, Germany

Prof. O. G. Schmidt
Center for Advancing Electronics Dresden
Dresden University of Technology
01062 Dresden, Germany

DOI: 10.1002/adma.201503696

Combining mechanical adaptivity of soft actuators with the imperceptibility of microelectronics paves the way toward an entirely new class of devices–smart biomimetics. Smart biomimetics can mechanically adapt to and deterministically impact the environment electrically or mechanically. Foreseeable applications of this technology are far reaching. At the large scale, biomimetic microelectronics can assess the electrical activity of the brain[13] and the heart[14] in conformable and portable NeuroGrids, as well as the electrophysiological processes acting as a component of catheters[11] and artificial skins.[10,15] At the microscale, smart biomimetics bear great potential to impact the neurology and regenerative medicine by offering neuronal cuff-type implants[16,17] with unmatched functionalities. Due to the inherent ability to self-assemble, biomimetic microelectronics can be firmly yet gently attached to a biological tissue enabling enclosure of, e.g., nervous fibers, or guiding the growth of neuronal cells during regeneration (**Figure 1**a). The integrated electronics enables stimulating the biological tissue[18] and monitoring the healing process.[19] Upon external stimulation, e.g., after healing, the cuff can be opened, releasing thus the nervous tissue with minimal invasivity.

Here, we realize mechanically adaptive microchannels of cuff-type implant with integrated high-performance microelectronics including signal amplifiers and logic circuitry based on indium gallium zinc oxide (IGZO) transistors.[12] The active electronic devices are fabricated on a polyimide support capping a hydrogel-based stimuli-responsive layer. The swelling state of the hydrogel can be affected by tailoring the environmental conditions, including solution composition and pH. This provides full control over the shape of the device, which can be deterministically set in a planar or bent state, as well as self-assembled into a Swiss roll-like microtube (Figure 1b) with a tunable diameter (Figure 1c) ranging from 50 µm (Figure 1c, top inset) to 1 mm (Figure 1c, bottom inset). Inorganic rolled-up microtubes less than 10 µm in diameter have previously been shown to act as ultracompact microfluidic channels with fully integrated electrodes and field effect transistors, able to detect polar and ionic fluids down to subnanomolar concentrations, sense single cancer cells, and guide neuronal outgrowth.[20–22] Medical applications of such tubular architectures have been envisioned for topographically mediated nerve growth, tissue engineering, and regeneration.[22] The opportunity to open/close such microscale devices upon external stimulation brings these applications closer to reality and is particularly appealing for neuronal cuff implant applications to enclose and guide the growth of nervous fibers with a typical size of 10–50 µm.[18] The achieved device diameters of 50 µm are at least two orders of magnitude smaller compared to the state-of-the-art neuronal cuff implants.[23] We prove biocompatibility of the polymeric platform and demonstrate differentiation and guided

ADVANCED MATERIALS
www.advmat.de
www.MaterialsViews.com

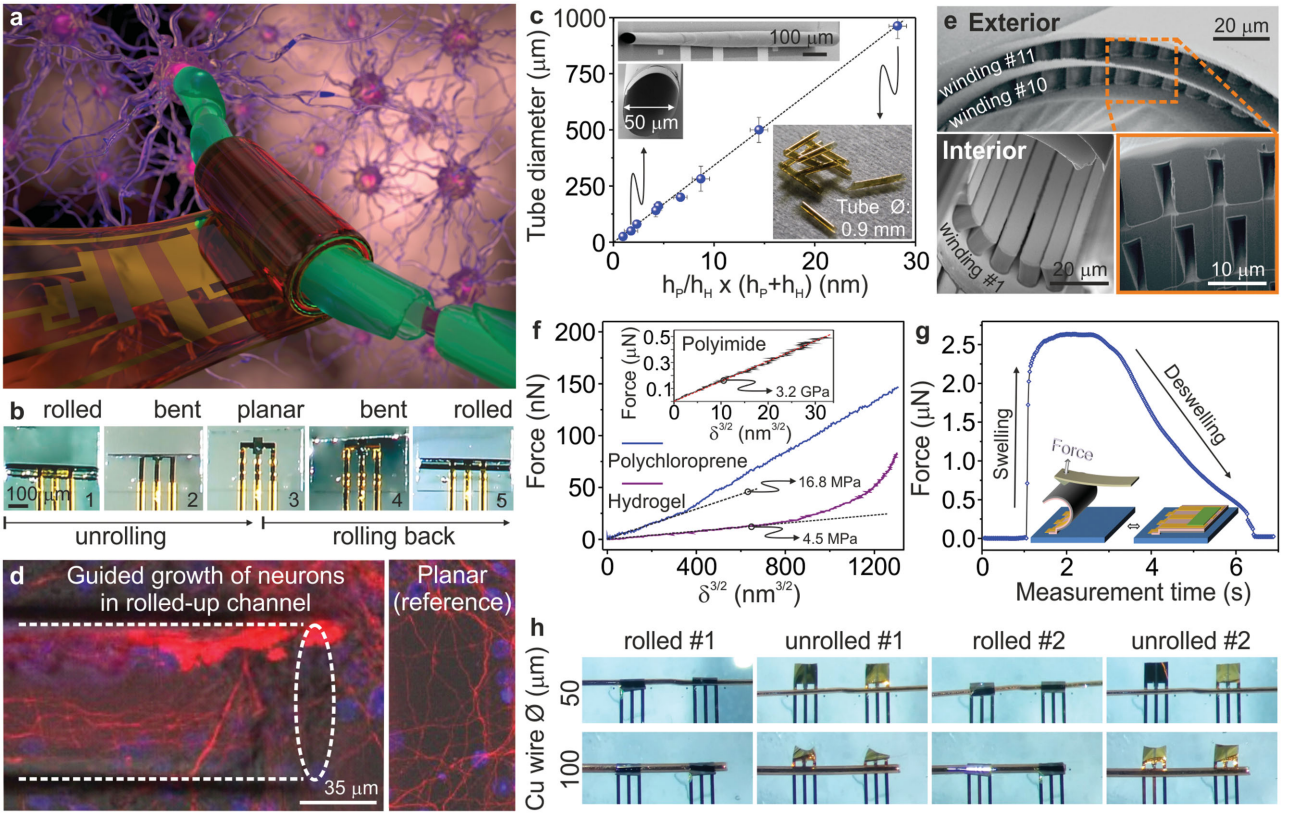

Figure 1. Biomimetic microelectronics for cuff implants: mechanical properties. a) Conceptual image. Biomimetic microelectronics bear great potential to offer neuronal cuff-type implants with unmatched mechanical and electrical functionalities. b) The shape of the device can be deterministically chosen to be planar, bent, or self-assembled into a Swiss roll like microtube. c) The diameter of the microtube can be tuned by adjusting the thicknesses of the hydrogel layer, h_H, and the stiff polyimide reinforcement layer, h_P. Optical micrographs of the Swiss roll tubes with a diameter of 50 and 900 µm are shown as top and bottom insets, respectively. d) Guided growth of differentiated neurons in the channel formed by a microtube. e) Regular openings (ribbons) with the cross-section area of 3×6 µm^2 patterned in each winding of the Swiss roll architecture. f) Force–distance curve measured for different polymeric layers using AFM. The study is carried out on polymers with the same thickness as the functional stack used for the self-assembly. g) Change of the force measured using AFM upon self-assembly of the devices. The total radial pressure imposed by the device upon the self-assembly process is about 600 Pa. h) Hooking up several devices to Cu wires with a diameter of 50 µm (top row) and 100 µm (bottom row); see Movies 1 and 2 (Supporting Information), respectively. The rolled/unrolled state of the devices can be controlled by adjusting the content of isopropanol in the water solution.

outgrowth of neural stem cells from the cortex region of E14 mouse embryonic brains in the channels formed by the microtubes (Figure 1d and **Figure 2**). By patterning the polymeric spacer between neighboring windings of the Swiss roll like architecture, we achieve regular openings with a cross-section area of 3×6 µm^2 (Figure 1e) potentially enabling the guidance of individual neuronal fiber and single axons, which possess typical diameters in the micrometer range.[18] At the same time, the elasticity of the polymeric layer forming the interior of the channel is about 17 MPa, which matches the elasticity of the protective tissues of the central nervous system, in line with the requirements for in vivo implants.[3,23] The total radial pressure imposed by the device upon the self-assembly process is about 600 Pa, which is well below the harm limit of 1300 Pa characteristic for nerves and axons.[24] The Swiss roll geometry with multiple windings allows the device to adjust to the dimensions of the nerves during their life circle, reducing the probability of a compression trauma.[25,26] The small thickness of the polymers of less than 1 µm prevents the IGZO electronics from degradation upon severe mechanical deformations, e.g., bending to a curvature radius of 25 µm. This is by far the smallest reported bending radius imposed on the entire circuit containing amplifiers and logic devices. Even in the most bent state, the signal amplifiers and the advanced logic including inverters (NOT gates) and universal (NAND) gates remain fully intact and maintain their functionality. The threshold voltages of individual transistors remain below 1 V and the maximum saturation current approaches remarkably high values of 1 mA. In the assembled state, analog amplifiers possess a unity gain frequency of 30 kHz. We applied the integrated electronics to detect ionic signals from 10 pL of phosphate buffered saline (PBS) solution repeatedly pushed in the channel, demonstrating mV polarization response of the IGZO transistor. With this performance, the platform can be readily used for monitoring the action potential of ionic axons. Furthermore, the demonstrated possibility to integrate the high-performance amplifiers at the location where the signals of interest are acquired allows increasing the signal-to-noise ratio, which is of strong advantage for the diagnostic of neuronal activity.[27–29]

Fabrication of microchannels with integrated electronics: To realize mechanically active, stimuli-responsive, and high-performance IGZO microelectronics, we formulated and

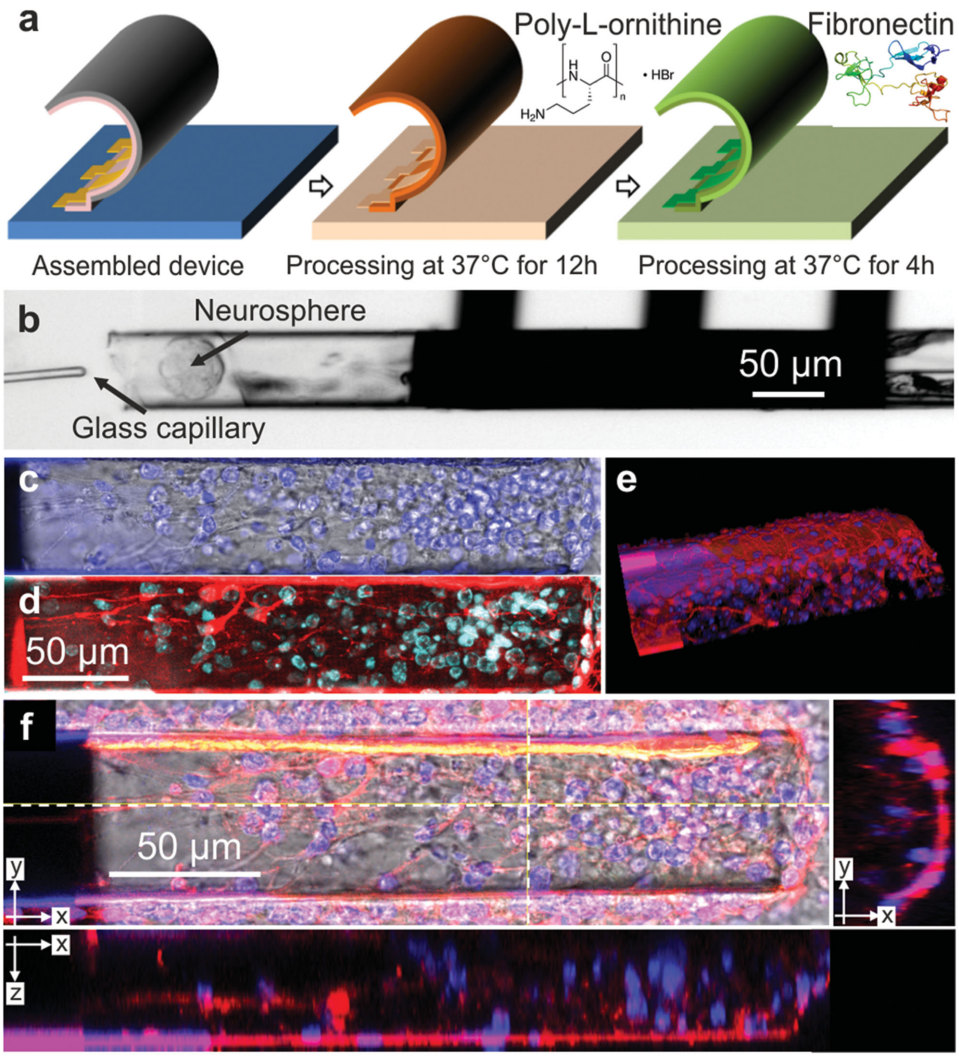

Figure 2. Biocompatibility and guidance of neurons. a) Schematic of the bioactivation of an already assembled Swiss roll microtube. b) The neurosphere is placed inside the microtubular architecture. c,d) *z*-stack intensity projections of one-half of the device populated with immunofluorescently labeled neurons (red). Cell nuclei are depicted in blue/cyan. e) 3D reconstruction of one half of the device that is populated with immunofluorescently labeled cells (see also Movie 3 in the Supporting Information). Cell bodies of neurons are stained in red and cell nuclei in blue. f) Cut views (positions indicated by white dashed lines) through a *z*-scan of one half of the device populated with cells. Neurons are immunofluorescently labeled in red, cell nuclei are stained in blue.

synthesized novel photopatternable polymers allowing a full-scale microelectronic fabrication process including multistep lithography, depositions, as well as dry and wet etching. The polymeric layer stack includes a water-soluble metal–organic sacrificial layer (thickness: 175 nm), a highly cross-linked hydrogel-based swelling layer (thickness: 200 nm), as well as a stiff polyimide film (thickness: 500 nm) acting as a single layer reinforcement for the stimuli-responsive hydrogel. Details on the synthesis can be found in the Experimental Section; see also Figure S1 in the Supporting Information. This polymeric functional stack with a total thickness of less than 1 µm is processed onto 80×80 mm^2 glass substrates using optical lithography to realize the predefined locations that will host the electronics (Figure 1b and **Figure 3**a). The IGZO-based individual thin-film transistors (Figure S2, Supporting Information), the key digital logic elements, i.e., inverters (NOT gates) and universal (NAND) gates, as well as the analog amplifiers with a total thickness of the stack of about 80 nm are prepared onto the lithographically predefined locations with a typical lateral size of 800×500 µm^2 and 2000×1000 µm^2. The circuitry is locally protected by the 40 nm thick photopatternable polychloroprene-based capping layer.

By placing the substrate into a neutral aqueous solution of sodium diethylenetriaminepentaacetic acid (DTPA), the sacrificial layer is selectively removed leading to the free standing polymeric membrane with embedded IGZO electronics. The entire membrane is anchored at one edge to the handling glass substrate. The stiff polyimide reinforcement layer allows fixing the lateral dimensions of the devices at the top surface of the hydrogel. In the water solution, the hydrogel swells from below and generates thus the differential mechanical stress in its thickness that results in the upward bending of the entire architecture.[30–32] Ultimately, the initially planar device will be

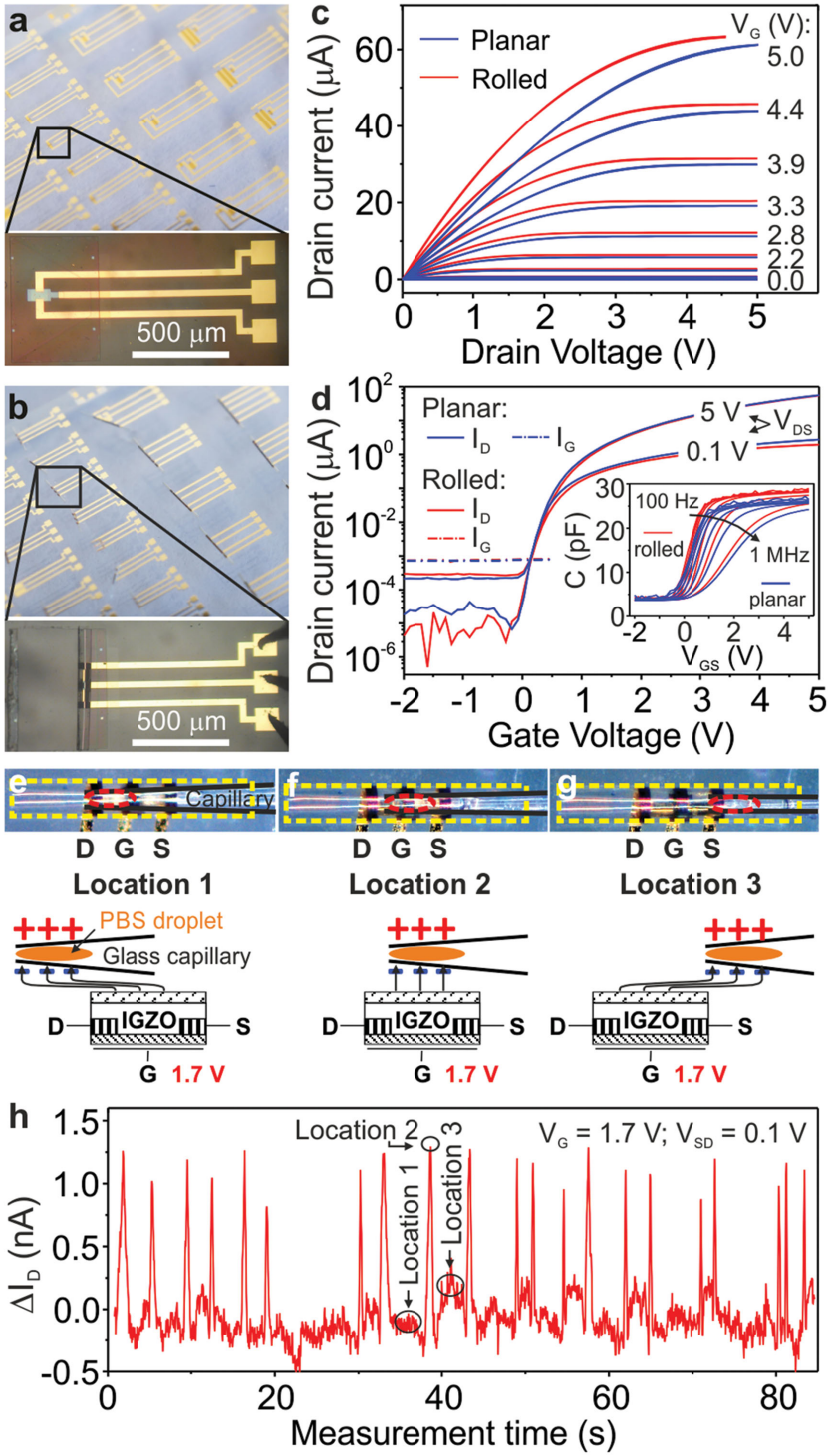

Figure 3. Electrical performance of transistors and measurement of the ionic solution. a) Array of planar IGZO devices. The inset in (a) shows an individual transistor device with a channel width of 50 µm and length of 60 µm before the self-assembly process. b) Array of self-assembled IGZO transistors, logic elements, and amplifiers. The inset in (b) shows a tubular architecture accommodating one IGZO transistor device with the channel along the tube axis. c) Output and d) transfer characteristics of the transistor device shown in (a) and (b) in planar (blue curves) and assembled (red curves) states. Inset in (d) shows the *C*–*V* characteristics. e–h) Mimicking the measurement of the polarization/depolarization of neural microconduits: a droplet containing the PBS solution is located in a glass microcapillary and then inserted into the microchannel comprising an IGZO transistor (channel width: 50 µm; channel length: 40 µm) oriented along the tube axis. The location of the droplet with PBS is adjusted to be e) before, f) above, or g) after the gate electrode (see Movie 4 in the Supporting Information). Schematics in (e–g) show the modification of the electric field of the gate electrode due to the induced double layer in the droplet with the ionic liquid. h) The variation of the drain current of the transistor while moving the charged droplet with PBS multiple times above the location of the gate electrode.

transformed into a compact Swiss roll like architecture composed of one or several windings and with a lithographically defined length in the range of some millimeters (Figure 1c).

The fabrication platform allows the realization of arrays of mechanically active microchannels with integrated high-performance IGZO microelectronics over the entire 80 × 80 mm^2 glass substrates with a yield of more than 90% derived from 500 devices.

Elastic moduli of the device: The mechanical properties of the polymers influence the self-assembly process and determine the final geometry of the device, e.g., diameter and number of windings. The elastic modulus of each polymeric layer with the thicknesses as in the functional stack was determined by measuring the force–distance curve with an atomic force microscope (AFM) tip indenting the layer (Figure 1f), accordingly to the routine proposed by Rosso et al.[33] The data was fitted to the Hertzian model[34] (see the Experimental Section for details) and the Young's modulus was determined by analyzing the slope of the linear part of the force–distance curve. We achieve a Young's modulus of the materials of 16.8 MPa for the capping polychloroprene layer, 4.5 MPa for the hydrogel layer, and 3.2 GPa for the stiff polyimide layer. The Young's modulus of the outer hydrogel layer and the inner polychloroprene layer is in the same range as the modulus of the protective tissues of the central and peripheral nervous system, namely dura and pia matter (20 MPa and 2.3 MPa, respectively), as well as the nerves itself (elastic modulus of the sciatic nerve is about 40 MPa).[35–37] This renders our microchannels mechanically biocompatible for in vivo applications.

Tailoring diameters of the microchannels: The diameter of the tubular structures can be tuned over a wide range, by adjusting the thicknesses of the individual polyimide, h_P, and hydrogel, h_H, layers. The chosen thicknesses determine the differential strain generated in the hydrogel layer upon immersing it into a solvent. Furthermore, the lithographically defined dimensions of the initial planar layout and the resulting

diameter of the microtube determine the number of windings in the Swiss roll architecture. For instance, the self-assembly process of the initial planar device with an area of 800×400 μm^2 consisting of the stack of 500 nm thick polyimide and 200 nm thick hydrogel rolls up into a tube with a diameter of 50 μm, leading to a Swiss roll architecture with 2.5 windings (Figure 1c, top inset). To realize a tube of 500 μm diameter, the thickness of the polyimide layer should be increased to 1400 nm, while the hydrogel layer should become thinner with $h_H = 150$ nm.

The possibility to tune the inner diameter of the tubes from 50 μm to ≈1 mm allows using these architectures as regenerative cuff implants to guide the growth of nerves and nervous fasciculus. Here, we use neural stem cells from the cortex region of E14 mouse embryonic brains to demonstrate their guided growth in the self-assembled tubular channels. First, the tubes were functionalized with the extracellular matrix protein fibronectin to promote cell adhesion (Figure 2a). Neural stem cell neurospheres were gently triturated to produce cell clusters with dimensions comparable to the inner diameter of the microtubes. The neurospheres were then plated onto the samples in growth factor-containing cell culture medium and positioned inside the tubes with the glass capillary (Figure 2b). After one day, the medium was replaced by culture medium without growth factors to initiate differentiation. The cells were allowed to differentiate for up to 7 d in a humidified incubator at 37 °C and 5% CO_2. Every two to three days, 100×10^{-6} M dibutyryl cAMP was added to the medium. The neural stem cell did adhere and proliferate in the growth factor-supplemented medium and then differentiate into neurons in the absence of the growth factors, demonstrating the biocompatibility of the used material system. Optical imaging by an inverse confocal laser scanning microscope clearly demonstrates guided growth of neurons along the channel defined by the tube (Figure 2c–f and Movie 3, Supporting Information).

Small-sized multiple channels: The separate guidance of individual axons possessing diameters of about 0.5–10 μm,[18] as required for regenerative medicine, has not been accomplished yet due to the lack of cuff implants with appropriate dimensions. We realized such a template by lithographically defining 1D mesa structures directly on the top surface of the polymeric functional layer before the self-assembly process. Assembly of these devices bring the mesa array in contact with the back side of the hydrogel layer thus forming as many as 1600 channels with a characteristic cross-section of 3×6 μm^2 spanning all the way along the axis of the tube with a diameter of 250 μm and 11 windings (Figure 1e and Figure S3, Supporting Information).

Mechanical actuation: The hydrogel layer is responsive to the composition of the rolling solution. After being swollen in the aqueous solution in order to achieve rolled-up tubular architectures (Figure 1b1), the volume of the hydrogel layer can be reduced by adding isopropanol to the solution in vitro. A high concentration of isopropanol breaks the hydrogen bonds leading to the dehydration of the hydrogel. (The observed behavior is similar to the response of the PNIPAM hydrogels on ethanol.[38]) The shrinkage of the hydrogel results in the unrolling of the device (Figure 1b2), eventually transforming it into the original planar layout (Figure 1b3). Adding more water to the solution leads to the swelling of the hydrogel again initiating the self-assembly process (Figure 1b4,b5). This mechanical transformation of the device between the rolled and unrolled states can be performed repeatedly by controlling the amount of the isopropanol in the water solution.

The possibility to open/close the architecture upon external stimulation allows an automatic attachment and release of a device to/from an object of interest in a biomimetic fashion. We demonstrated this feature by hooking up several devices to Cu wires with a diameter of 50 μm (Figure 1h, top row) and 100 μm (Figure 1h, bottom row); see Movies 1 and 2 (Supporting Information), respectively. All devices in the array behave similarly, indicating good homogeneity of the mechanical properties from device to device. To unroll the devices, we added 20 mL of isopropanol to the initial water solution. The consecutive roll-up process is initiated by adding 100 μL of water solution to the solvent. In total, we performed 7 open–close cycles with the same device. No degradation of the shape of the self-assembled devices was observed.

The polymeric layer stack is designed in a way such that it can be actuated upon drying the isopropanol from the water solution. The isopropanol is a standard agent used in medicine for external disinfection. The possibility to open the device by immersing it into an isopropanol and, after drying the alcohol, to permanently lock the device around an object, e.g., nerves or neurons when exposed to the humid environment of the human body, bears great potential for less invasive yet gentle attachment of this cuff-type implant upon medical treatment.

Radial pressure upon actuation: Gentle attachment of the device to soft biological tissues, e.g., neural tissue, is of crucial importance to avoid implant-driven damages. Hence, forces exerted by the device should be quantified. We used AFM to estimate the mechanical radial force and pressure produced by the device upon actuation. The AFM tip is placed on top of the dry planar polymeric stack. Then, the system is exposed to 100% humid air, resulting in the self-assembly of the device (Figure 1g). By monitoring the force exerted at the edge of the stack in a defined area of 47×47 μm^2, we estimated the edge force of about 2.6 μN (Figure 1g). By recalculating to the total lateral area of the device of 800×500 μm^2, we extracted a radial force of 0.24 mN, which is equivalent to about 600 Pa (6.1 cm H_2O, 4.5 mm Hg, ≈60 kg m^{-2}). The value is at least two times smaller than the compressive harm limit of axons[24,26,39] and two orders of magnitude lower than compressive irreversible injury of the spinal root nerve.[40,41]

Electric performance of compact transistors: Shaping the initially planar IGZO electronics (Figure 3a) into compact tubular architectures (Figure 3b) even down to diameters of 50 μm does not affect their functionality. Detailed investigation of single transistors before and after self-assembly shows only minor impact on the output characteristics, and almost no variation in the transfer characteristics independent of the orientation of the channel with respect to the tube axis (Figure 3c,d and Figure S4 and Table S1, Supporting Information). The threshold voltages remain below 1 V (Figure 3d), and the maximum saturation current approaches a remarkably high value of 1 mA for the drive transistors with the channel of 525 μm in width and 15 μm in length. The devices reveal extremely small subthreshold swing in the range of 165 mV dec^{-1} and ON/OFF current ratio of 10^5. The capacitance of the transistor is slightly increased after rolling (Figure 3d, inset) due to the overlap capacitance of the electrodes between the windings of the

assembled device. This finding indicates only partial screening of the gate electric field by the IGZO semiconductor, in turn enabling detection of external electric fields from the top side of the transistor. This, so called, frontend detection and amplification is an important feature to enhance the sensitivity of the acquisition system.[28,29]

Measurement of the ionic solution: Amplification of the signal directly at the measurement location is commonly used in microelectronics to improve the signal-to-noise ratio. However, state-of-the-art neuronal implants do not contain active electronics directly at the measurement location. Hence, transferring the signal to the conditioning electronics via cable connections decreases the sensitivity of the entire system and limits the possibility to assess tiny electrical signals stemming from e.g., nerves and axon fibers of neurons.

We overcome this limitation by relying on the possibility of the frontend detection and amplification offered by the rolled-up high-performance IGZO transistors. To mimic the measurement of the polarization/depolarization of the neural microconduit, we assembled a demonstrator (Figure S5, Supporting Information) where a 30 µm long droplet containing the ionic liquid of 10 pL PBS (as purchased, Gibco Invitrogen, Germany) is located in a glass microcapillary with an inner diameter of 20 µm (Figure 3e–g). The dimensions of the capillary are adjusted in a way that it can be placed inside the assembled microtubular device comprising an IGZO transistor by means of a micromanipulator (Movie 4, Supporting Information). For the measurement, we applied a 0.1 V drain–source voltage; the gate electrode was biased to 1.7 V. By monitoring the transistor response, we can clearly distinguish the events when the droplet with the ionic liquid passes over gate electrode, as reflected by the appearance of the peaks in the *I–V* characteristic (Figure 3h). The mechanism is as follows: the electric stray field of the gate electrode polarizes the ionic solution resulting in the formation of a double layer (see schematics in Figure 3e–g and Figure S6a, Supporting Information), thus altering the electric field in the IGZO semiconductor. The difference in the drain–source current of about 1 nA is measured for the cases when the droplet is present and absent at the location of the gate electrode (Figure 3h). Taking into account the transfer characteristics, this change of the drain–source current corresponds to a ≈20 mV variation in gate voltage (Figure S6b, Supporting Information). Such value would be sufficient to detect action potentials of ionic axons in the direct vicinity of the transistor.[42] We note that the device is not sensitive to the nonionic solutions (see control experiment performed on nonionic sugar solution in Figure S7 in the Supporting Information).

Compact analog and digital electronic circuits: Fabrication of complex logic circuits on mechanically active polymers, also including shape-memory[3] or electroactive polymers,[43] is attractive for electrical channel multiplication on the microscale, as well as for multicontact self-confined neural cuff implants. Digital electronics combined with analog circuits have great potential for interfacing and monitoring applications in regenerative medicine. Preamplification and multiplexing could potentially allow the use of a low number of interconnects, drastically below the several tenths or even hundreds of conductors required in state-of-the-art devices. Therefore, in addition to the individual transistors, we fabricated two basic elements, namely inverter (**Figure 4**a–f) and NAND (Figure 4g–j) gates.

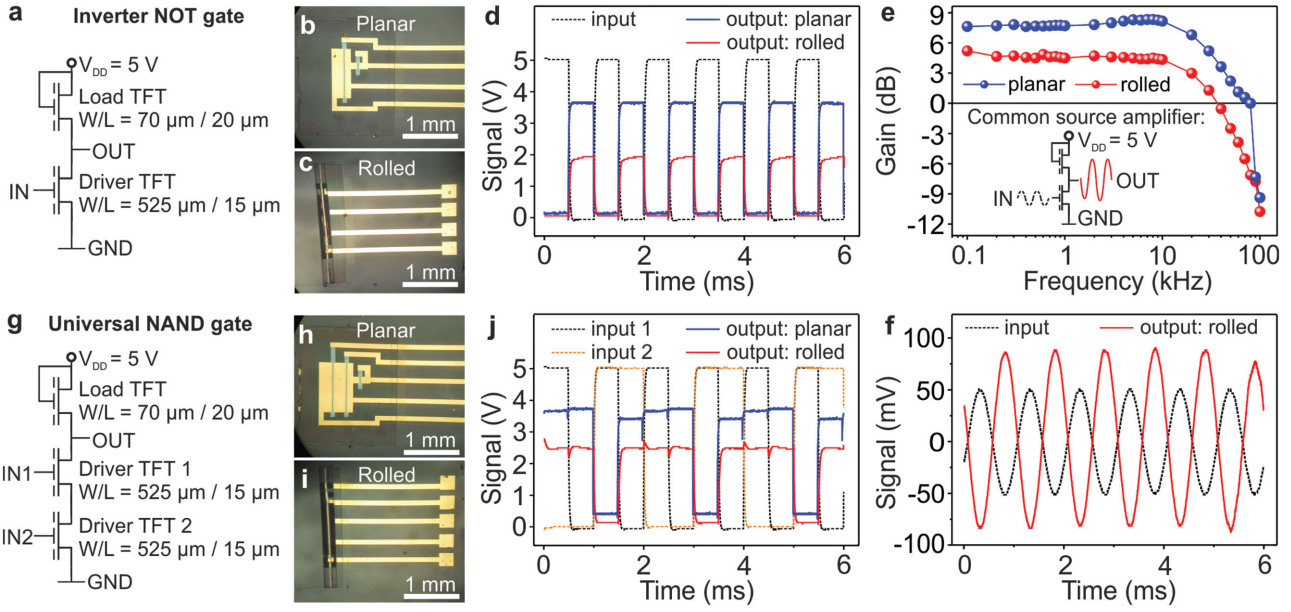

Figure 4. Compact logic elements. a) Schematic of the circuit realization of the inverter (NOT gate). Optical micrograph of the inverter device b) before and c) after the self-assembly process. d) Time evolution of the output signal of the planar (blue line) and rolled-up (red line) inverter device when excited with a square-wave signals with amplitude of 5 V. e,f) NMOS inverter circuit can be successfully used as a common source amplifier revealing a unity gain frequency of 30 kHz. Bias point: 1.1 V. Schematic of the circuit realization of the common source amplifier is shown as inset in (e). g) Schematic of the circuit realization of the universal (NAND) gate. Optical micrograph of the NAND gate h) before and i) after the self-assembly process. j) Time evolution of the output signal of the planar (blue line) and rolled-up (red line) NAND gate devices when excited with the two square-wave signals of 5 V, which are twice different in frequency.

An inverter (Figure 4a) is a NOT gate in the digital logic but at the same time its circuit realization is similar to the common source amplifier (Figure 4e, inset). Hence, it can be used as an analog amplifier as well. The NOT gate is formed by a drive transistor with a channel width and length of 525 µm and 15 µm, respectively, loaded by a transistor in diode configuration with a channel geometry of 70 µm in width and 20 µm in length. The response of the planar NOT gate (before self-assembly, Figure 4b) to the square-wave input signal with a 5 V amplitude produces an inverted output voltage of 3.8 V. After being assembled into a compact Swiss roll architecture with a diameter of 50 µm possessing 2.5 windings (Figure 4c), the same element reveals signal inversion with an output voltage of 2 V, slightly lower compared to the planar device (Figure 4d). Excitation of the rolled-up inverter with a low amplitude harmonic signal demonstrates the possibility to employ the NOT gate as a common-source amplifier operating at input signals with frequencies up to 30 kHz (Figure 4e,f).

The NAND gate is a universal gate (Figure 4g–i), enabling fabrication of more complex logic circuits. The NAND gate is formed by two drive transistors with a channel width and length of 525 µm and 15 µm, respectively, connected in series and loaded by a transistor with the channel geometry of 70 µm in width and 20 µm in length. To demonstrate its operation, the NAND gate was subjected to two meander shape signals of 5 V, which are different by a factor of two, both in frequency and pulse length (Figure 4j). The shape of the output signal is characteristic for the NAND gate revealing slightly lower output voltages of 3.8 V for the planar structure and 2.5 V for the rolled-up devices (Figure 4j).

In conclusion, we realized mechanically adaptive microchannels with integrated microelectronics, including signal amplifiers and logics based on high-performance IGZO transistors. The microelectronic devices were fabricated on a 1 µm thick stimuli-responsive polymeric platform. This provides full control over the shape of the device, which can be deterministically chosen to be planar, bent, or self-assembled into a Swiss roll like microtube with a tunable diameter down to 50 µm. The small thickness of the polymer stack prevents the electronics from degradation upon severe mechanical deformations, e.g., bending to a curvature radius of about 25 µm. The elasticity of the inner polymeric layer is 17 MPa, which matches the elasticity of the protective tissues of the central and peripheral nervous system. We prove biocompatibility of the polymeric platform and demonstrate differentiation and guided growth of the neural stem cells in the channels formed by the microtubes. The integrated microelectronics allows monitoring the presence of tiny amounts of ionic liquids in the channel, mimicking the detection of polarization/depolarization processes in neural microconduits. Furthermore, the demonstrated possibility to integrate high-performance amplifiers at the location where the signals of interest are acquired allows increasing the signal-to-noise ratio, which is of strong advantage for brain diagnostics.

Our biomimetic microtubes constitute a major step toward 3D-assembled microelectronics for neural network regeneration, monitoring, and stimulation. The ability to assemble polymers into 3D microarchitectures upon external stimulation and matched mechanical properties should be of great value, reducing the injury of biological tissue and promoting biocompatibility.

Experimental Section

Polymeric Layer Stack: Synthesis and preparation of the polymeric layer stack,[44,45] including adhesion and sacrificial layers as well as strained bilayers, is presented in the Supporting Information.

Fabrication of IGZO Electronics: In a single process on the same substrate, we prepared individual transistors and more complex devices including logic elements and amplifiers. The circuit design is based on NMOS technology using IGZO thin-film transistors. All geometrical parameters have been optimized using a SPICE simulation.[46] Details on the sample fabrication are provided in the Supporting Information. We tested more than 100 individual devices before and after the self-assembly process. All devices were operational and revealed the following parameter spread: the threshold voltage averaged over all measured devices before and after rolling was (0.60 ± 0.15) V and (0.66 ± 0.17) V, respectively. The mobility was estimated to be (17.0 ± 4.7) $cm^2\ V^{-1}\ s^{-1}$ and (18.1 ± 5.1) $cm^2\ V^{-1}\ s^{-1}$ for planar and self-assembled devices, respectively.

Protecting Layer: Before initiating the self-assembly process, all active areas of the structures were protected with photopatternable polychloroprene. Details on the synthesis of the photopatternable polychloroprene layer are in the Supporting Information.

Self-Assembly Process: The planar devices were rolled up into 3D tubular architectures by selectively etching the sacrificial layer in the solution of 0.5 M sodium DTPA (Alfa Aesar, UK). After the etching process, the structures were washed in DI water. To initiate the rolling process, water was almost completely exchanged with isopropanol in proportion 1:5. Then, the substrate was removed from the solution and dried under ambient conditions.

By tailoring the pH and the composition of the solution, we can tune the self-assembly process in the way to stabilize the membrane in the released state from substrate planar state or in assembled (tubular) state. To release the device without the assembly into a tube, the etching of the sacrificial layer should be done in a water solution at pH below 7. Here, the best results were obtained at a solution pH 5 adjusted by acetic acid. Vice versa, the self-assembly of the device into a Swiss roll architecture is done in the solution with pH 8 adjusted by a sodium hydroxide. To fix the shape of the device, the tubular architectures are dried in 80% v/v water–alcohol mixture under ambient conditions.

Sample Functionalization: For sterilization, samples were carefully rinsed with 70% ethanol (VWR) for at least 15 min. They were then functionalized with the extracellular matrix protein fibronectin to promote cell adhesion. Therefore, the samples were incubated overnight at 37 °C in a 15 mg mL^{-1} poly-L-ornithine (Sigma-Aldrich Co. LLC, Germany) solution in Dulbecco's phosphate-buffered saline DPBS (Gibco/Invitrogen, Germany), washed three times with DPBS and then incubated with 0.02 mg mL^{-1} fibronectin (Sigma-Aldrich Co. LLC, Germany) in DPBS at 37 °C for 3 h. The samples were carefully rinsed with DPBS solution and stored at 4 °C until used.

Cell Culture: Neural stem cells from the cortex region of E14 mouse embryonic brains were a generous gift of A. Storch (Neuroregeneration/Neurodegeneration, Dresden Division of Neurodegenerative Diseases, University Hospital Carl Gustav Carus, Dresden) and maintained as neurosphere culture in a 2:1 mixture of high glucose Dulbecco's modified Eagle medium (Sigma-Aldrich Co. LLC, Germany) and Ham's F-12 Nutrient Mixture (Gibco/Invitrogen, Germany), complemented with 2% B-27 supplement (50x, Gibco/Invitrogen, Germany), 1% penicillin/streptomycin (10 000 U mL^{-1}, Gibco/Invitrogen, Germany), and 20 ng mL^{-1} each of Egf and Fgf-2 (Sigma-Aldrich Co. LLC, Germany). Cultures were kept in a humidified incubator at 37 °C and 5% CO_2. Fresh growth factors were provided every two to three days and the neurospheres were separated every 5–7 d by gentle trituration and replating in low-adhesion cell culture flasks (Greiner Bio-One, Germany).

Differentiation Experiments: Neural stem cell neurospheres were gently triturated one day prior to utilization to produce cell clusters with the size comparable to the inner diameter of the tubular architecture. The neurospheres were then plated onto samples in growth factor-containing cell culture medium and positioned inside the microtubes with the help of a PatchMan NP 2 micromanipulation system (Eppendorf, Germany). After 1 d, the medium was replaced by culture medium without growth factors to initiate differentiation. The cells were allowed to differentiate for up to 7 d in a humidified incubator at 37 °C and 5% CO_2. Every 2 to 3 d, 100×10^{-6} M dibutyryl cAMP (Sigma-Aldrich Co. LLC, Germany) was added to the medium.

Mechanical Properties: The AFM instrument Veeco Dimension 3100 is used to assess the elastic modulus and measure the radial force produced by the device upon actuation. All the measurements started with the indentation of an oxidized silicon surface to determine the sensitivity of the tip. This information is needed to determine the sensitivity of the AFM tip in order to calculate the indentation depth and the force in soft polymers. Then, the force distance curves are plotted in a Hertzian scale of indentation depth $\delta^{3/2}$. The linear part of the indentation curve is fitted to the Hertzian model $F = \frac{4E}{3(1-\nu^2)}\sqrt{r}\delta^{\frac{3}{2}}$ to determine the Young's modulus, E, where $\nu = 0.5$ is a Poisson ratio and r = 7 nm is a tip curvature radius. We tested 200 nm thick hydrogel layer, 500 nm thick polyimide layer, protecting 40 nm thick polychloroprene layer, and bulky piece of polydimethylsiloxan 1:10 (PDMS). We estimate the Young's modulus of 16.8 MPa for the capping polychloroprene layer, 4.5 MPa for the hydrogel layer, 3.2 GPa for the stiff polyimide layer, and 2.6 MPa for PDMS (Figure S8, Supporting Information). The latter is used as a reference.

Furthermore, we use AFM to estimate the mechanical radial force and pressure produced by the device upon its actuation. AFM tips (OMCL-AC160TS-R3) with the spring constant of 26 N m^{-1} are placed on top of the dry planar rectangular shaped 47×47 μm^2 bilayer of hydrogel and polyimide. Then, the sample is exposed to 100% humid air resulting in the actuation of the device. The force of 2.6 μN produced by the edge of the structure was recalculated to the device with the footprint of 800×500 μm^2 resulting in a value of 0.24 mN in radial direction. This is equivalent to about 60 kg of weight distributed over 1 m^2 (600 Pa).

Supporting Information

Supporting Information is available from the Wiley Online Library or from the author.

Acknowledgements

D.K. and N.M. contributed equally to this work. The authors thank K. Crien and I. Fiering (IFW Dresden) for the deposition of oxides and metal layer stacks and Ch. Vogt (ETH Zürich) for optical characterization of the thin film devices. The support in the development of the experimental setups from the Research Technology Department of the IFW Dresden and the clean room team headed by Dr. S. Harazim (IFW Dresden) is greatly appreciated. The authors thank Dr. L. Ionov and Dr. G. Stoychev (IPF Dresden) for valuable discussions. O.G.S appreciates fruitful discussions with J.P. Spatz (Max-Planck-Institute for Intelligent Systems). The authors are grateful to A. Storch (University Hospital Carl Gustav Carus, Dresden) for providing neurosphere stem cell cultures. The authors also thank the light microscopy facility of the BIOTEC/CRTD (TU Dresden) for excellent support. This work is financed in part via the European Research Council within the European Union's Seventh Framework Programme (FP7/2007-2013)/ERC grant agreement no. 306277, European Commission within the European Union's seventh framework program FLEXIBILITY/Grant No. 287568 and DFG Research Group FOR1713.

Received: July 30, 2015
Revised: August 20, 2015
Published online: September 23, 2015

[1] S. Schuhladen, F. Preller, R. Rix, S. Petsch, R. Zentel, H. Zappe, *Adv. Mater.* **2014**, *26*, 7247.
[2] R. Yoshida, T. Ueki, *NPG Asia Mater.* **2014**, *6*, e107.
[3] J. Reeder, M. Kaltenbrunner, T. Ware, D. Arreaga-Salas, A. Avendano-Bolivar, T. Yokota, Y. Inoue, M. Sekino, W. Voit, T. Sekitani, T. Someya, *Adv. Mater.* **2014**, *26*, 4967.
[4] R. Fernandes, D. H. Gracias, *Adv. Drug Deliv. Rev.* **2012**, *64*, 1579.
[5] Y. Qiu, K. Park, *Adv. Drug Deliv. Rev.* **2012**, *64*, 49.
[6] L. Ionov, *Mater. Today* **2014**, *17*, 494.
[7] R. M. Erb, J. S. Sander, R. Grisch, A. R. Studart, *Nat. Commun.* **2013**, *4*, 1712.
[8] K. Malachowski, M. Jamal, Q. Jin, B. Polat, C. J. Morris, D. H. Gracias, *Nano Lett.* **2014**, *14*, 4164.
[9] K. Fukuda, Y. Takeda, M. Mizukami, D. Kumaki, S. Tokito, *Sci. Rep.* **2014**, *4*, 3947.
[10] M. Kaltenbrunner, T. Sekitani, J. Reeder, T. Yokota, K. Kuribara, T. Tokuhara, M. Drack, R. Schwödiauer, I. Graz, S. Bauer-Gogonea, S. Bauer, T. Someya, *Nature* **2013**, *499*, 458.
[11] D.-H. Kim, N. Lu, R. Ghaffari, J. A. Rogers, *NPG Asia Mater.* **2012**, *4*, e15.
[12] G. A. Salvatore, N. Münzenrieder, T. Kinkeldei, L. Petti, C. Zysset, I. Strebel, L. Büthe, G. Tröster, *Nat. Commun.* **2014**, *5*, 2982.
[13] D. Khodagholy, T. Doublet, P. Quilichini, M. Gurfinkel, P. Leleux, A. Ghestem, E. Ismailova, T. Hervé, S. Sanaur, C. Bernard, G. G. Malliaras, *Nat. Commun.* **2013**, *4*, 1575.
[14] X. Strakosas, M. Bongo, R. M. Owens, *J. Appl. Polym. Sci.* **2015**, *132*, 41735.
[15] M. Ramuz, B. C.-K. Tee, J. B.-H. Tok, Z. Bao, *Adv. Mater.* **2012**, *24*, 3223.
[16] D. J. Chew, L. Zhu, E. Delivopoulos, I. R. Minev, K. M. Musick, C. A. Mosse, M. Craggs, N. Donaldson, S. P. Lacour, S. B. McMahon, J. W. Fawcett, *Sci. Transl. Med.* **2013**, *5*, 210ra155.
[17] I. R. Minev, P. Musienko, A. Hirsch, Q. Barraud, N. Wenger, E. M. Moraud, J. Gandar, M. Capogrosso, T. Milekovic, L. Asboth, R. F. Torres, N. Vachicouras, Q. Liu, N. Pavlova, S. Duis, A. Larmagnac, J. Vörös, S. Micera, Z. Suo, G. Courtine, S. P. Lacour, *Science* **2015**, *347*, 159.
[18] X. Navarro, T. B. Krueger, N. Lago, S. Micera, T. Stieglitz, P. Dario, *J. Peripher. Nerv. Syst.* **2005**, *10*, 229.
[19] D. Borton, M. Bonizzato, J. Beauparlant, J. DiGiovanna, E. M. Moraud, N. Wenger, P. Musienko, I. R. Minev, S. P. Lacour, J. del R. Millán, S. Micera, G. Courtine, *Neurosci. Res.* **2014**, *78*, 21.
[20] C. S. Martinez-Cisneros, S. Sanchez, W. Xi, O. G. Schmidt, *Nano Lett.* **2014**, *14*, 2219.
[21] D. Grimm, C. C. Bof Bufon, C. Deneke, P. Atkinson, D. J. Thurmer, F. Schäffel, S. Gorantla, A. Bachmatiuk, O. G. Schmidt, *Nano Lett.* **2013**, *13*, 213.
[22] B. S. Schulze, G. Huang, M. Krause, D. Aubyn, V. A. Bolaños Quiñones, C. K. Schmidt, Y. Mei, O. G. Schmidt, *Adv. Eng. Mater.* **2010**, *12*, 558.
[23] J. J. FitzGerald, N. Lago, S. Benmerah, J. Serra, C. P. Watling, R. E. Cameron, E. Tarte, S. B. McMahon, J. W. Fawcett, *J. Neural Eng.* **2012**, *9*, 16010.
[24] H. C. Powell, R. R. Myers, *Lab. Invest.* **1986**, *55*, 91.

[25] W. M. Grill, J. T. Mortimer, *J. Biomed. Mater. Res.* **2000**, *50*, 215.
[26] F. A. Cuoco Jr., D. M. Durand, *IEEE Trans. Rehabil. Eng.* **2000**, *8*, 35.
[27] D. Khodagholy, J. N. Gelinas, T. Thesen, W. Doyle, O. Devinsky, G. G. Malliaras, G. Buzsáki, *Nat. Neurosci.* **2015**, *18*, 310.
[28] S. Ingebrandt, C.-K. Yeung, M. Krause, A. Offenhäusser, *Eur. Biophys. J.* **2005**, *34*, 144.
[29] M. E. J. Obien, K. Deligkaris, T. Bullmann, D. J. Bakkum, U. Frey, *Front. Neurosci.* **2014**, *8*.
[30] V. Y. Prinz, V. A. Seleznev, A. K. Gutakovsky, A. V. Chehovskiy, V. V. Preobrazenskii, M. A. Putyato, T. A. Gavrilova, *Phys. E* **2000**, *6*, 828.
[31] O. G. Schmidt, K. Eberl, *Nature* **2001**, *410*, 168.
[32] S. Zakharchenko, E. Sperling, L. Ionov, *Biomacromolecules* **2011**, *12*, 2211.
[33] G. Rosso, I. Liashkovich, B. Gess, P. Young, A. Kun, V. Shahin, *Sci. Rep.* **2014**, *4*, 7286.
[34] B. Cappella, G. Dietler, *Surf. Sci. Rep.* **1999**, *34*, 1.
[35] D. Chauvet, A. Carpentier, J. M. Allain, M. Polivka, J. Crépin, B. George, *Neurosurg. Rev.* **2010**, *33*, 287.
[36] H. Ozawa, T. Matsumoto, T. Ohashi, M. Sato, S. Kokubun, *J. Neurosurg. Spine* **2004**, *1*, 122.
[37] G. Liu, Q. Zhang, Y. Jin, Z. Gao, *Neural Regen. Res.* **2012**, *7*, 2299.
[38] I. Alenichev, Z. Sedláková, M. Ilavský, *Polym. Bull.* **2007**, *58*, 191.
[39] G. G. Naples, J. T. Mortimer, A. Scheiner, J. D. Sweeney, *IEEE Trans. Biomed. Eng.* **1988**, *35*, 905.
[40] C. J. De Luca, L. J. Bloom, L. D. Gilmore, *Orthopedics* **1987**, *10*, 777.
[41] R. D. Hubbard, Z. Chen, B. A. Winkelstein, *J. Biomech.* **2008**, *41*, 677.
[42] B. P. Bean, *Nat. Rev. Neurosci.* **2007**, *8*, 451.
[43] D. Morales, E. Palleau, M. D. Dickey, O. D. Velev, *Soft Matter* **2014**, *10*, 1337.
[44] D. D. Karnaushenko, D. Karnaushenko, D. Makarov, O. G. Schmidt, *NPG Asia Mater.* **2015**, *7*, e188.
[45] D. Karnaushenko, D. D. Karnaushenko, D. Makarov, S. Baunack, R. Schäfer, O. G. Schmidt, *Adv. Mater.* **2015**,DOI:10.1002/adma.201503127.
[46] C. Zysset, N. Munzenrieder, L. Petti, L. Buthe, G. Salvatore, G. Troster, *IEEE Electron Device Lett.* **2013**, *34*, 1394.